

# SocialVAE: Human Trajectory Prediction using Timewise Latents

Pei Xu  
Clemson University  
South Carolina, USA  
peix@clemson.edu

Jean-Bernard Hayet  
CIMAT  
A.C., México  
jbbhayet@cimat.mx

Ioannis Karamouzas  
Clemson University  
South Carolina, USA  
ioannis@clemson.edu

**Abstract**—Predicting pedestrian movement is critical for human behavior analysis and also for safe and efficient human-agent interactions. However, despite significant advancements, it is still challenging for existing approaches to capture the uncertainty and multimodality of human navigation decision making. In this paper, we propose SocialVAE, a novel approach for human trajectory prediction. The core of SocialVAE is a timewise variational autoencoder architecture that exploits stochastic recurrent neural networks to perform prediction, combined with a social attention mechanism and backward posterior approximation to allow for better extraction of pedestrian navigation strategies. We show that SocialVAE improves current state-of-the-art performance on several pedestrian trajectory prediction benchmarks, including the ETH/UCY benchmark, the Stanford Drone Dataset and SportVU NBA movement dataset. Code is available at: <https://github.com/xupei0610/SocialVAE>.

## I. INTRODUCTION

Autonomous agents interacting with humans such as self-driving vehicles, service robots, and intelligent traffic control systems, have a strong demand for human behavior modeling and inference in order to meet both the safety and intelligence requirements. In recent years, with the rise of deep learning techniques, extracting patterns from sequential data for prediction or sequence transduction has advanced significantly in fields such as machine translation [1, 2], image completion [3, 4], weather forecasting [5, 6], and physical simulation [7, 8]. In contrast to works performing inference from regularly distributed data conforming to specific rules or physics laws, predicting human behaviors, e.g. speech, body pose and social-aware movement, still faces huge challenges, due to the complexity and uncertainty in the human decision making process.

In this work, we focus on the task of pedestrian trajectory prediction from a short-term historical observation. Traditional works predict pedestrian trajectories using deterministic models [9–13]. In real life, however, human navigation behaviors have inherent multimodal nature and exhibit lots of randomness. Even in the same scenario, there would be more than one trajectories that a pedestrian could take. Such uncertainty cannot be captured effectively by deterministic models, especially for long-term trajectory prediction with more aleatory influences introduced. Furthermore, individuals often exhibit different behaviors when facing similar scenarios. Such individual differences are decided by various stationary and dynamical factors such as crowd density and scene

lighting, weather conditions, social context, internal desires, personality traits, etc. As such, the complexity of human behaviors is hard to be consistently modeled by rule-based methods, which work under predetermined physical laws and/or social rules [9, 10, 12, 14]. To provide highly dynamic predictions, recent works [15–21] have promoted data-driven solutions based on generative models to perform stochastic predictions or learn the trajectory distribution directly. Despite impressive results, current approaches still face the challenge to provide high-fidelity prediction with a limited number of samples.

In this paper, we exploit recent advances in variational inference techniques and introduce a timewise variational autoencoder (VAE) architecture for pedestrian trajectory prediction. Similar to prior VAE-based methods [19–21], we rely on recurrent neural networks (RNNs) to handle trajectory data sequentially. However, our model introduces latent variables as stochastic parameters to condition the hidden dynamics of RNNs at each time step, in contrast to previous solutions that condition the prior of latent variables only based on historical observations. This allows us to more accurately capture the dynamic nature of human decision making. Further, to robustly extract navigation patterns from whole trajectories, we use a bidirectional RNN structure for posterior approximation rather than sequentially processing the trajectory from the start points only. To represent the scenario information with an arbitrary number of pedestrians during observation encoding, we develop an attention mechanism to encode neighbor states by considering the social features exhibited by the neighbors.

Overall, this paper makes the following contributions:

- We propose SocialVAE, a novel approach to predict pedestrian trajectory distributions conditioned on short-term historical observations. Our model relies on a timewise VAE architecture with a conditional prior and a posterior approximated from the whole trajectory bidirectionally. It uses an attention mechanism to capture the social influence from the neighboring agents.
- We experimentally show that SocialVAE can capture the multimodality of human navigation behaviors and accurately reason about human-human interactions.
- We achieve state-of-the-art performance on the ETH/UCY and SDD benchmarks and SportVU NBA movement dataset, bringing more than 15% and in certain benchmarks more than 50% improvement over existing trajectory prediction methods.

## II. RELATED WORK

Research in pedestrian trajectory prediction can be broadly classified into human-space and human-human models. The former focuses on predicting scene-specific human movement patterns [22–26] and takes advantage of the scene environment information, typically through semantic maps, for pedestrian trajectory prediction. In this work, we are interested in the latter, which performs trajectory prediction by using dynamic information about human-human interactions.

**Deterministic Models.** Traditional methods for modeling pedestrian movement in human-human interaction settings typically leverage hand-tuned mathematical models. They include rule-based approaches, social forces, velocity-obstacles, and energy-based formulations [9, 11–13, 27]. Such methods typically perform deterministic predictions and do not consider the uncertain nature of human behaviors, with many of them performing prediction only according to pedestrians’ immediate states without exploiting historical observations.

**Early Data-driven Models.** Statistical models based on observed data have also been used massively, in particular Gaussian processes (GP) [28–30]. By nature, they cope better with the uncertainties on overall trajectories but struggle to handle fine-grained variations due to social interactions. Moreover, performing inference with GPs scales badly with the number of observations.

**Generative Models.** In recent years, generative models for trajectory prediction have achieved impressive results. SocialLSTM [15] employs a vanilla RNN structure using long short-term memory (LSTM) units to perform trajectory prediction sequentially. SocialAttention [17] introduces an attention mechanism to capture neighbors’ influence by matching the RNN hidden state of each agent to those of its neighbors. SocialGAN [16], SoPhie [18] and SocialWays [31] use generative adversarial network (GAN) architectures. To account for the social interactions, SocialGAN proposes a pooling network to synthesize neighbor states, while SocialWays, as SocialAttention, adopts an attention mechanism but takes into account the neighbors’ social features rather than their corresponding RNN hidden states. While the GAN-based approaches use random noise as input to the model to generate stochastic results, PECNet [19], Trajectron [20] and Trajectron++ [21] rely on variational autoencoders (VAE) to predict trajectory distributions directly. These three methods use a conditional-VAE architecture [32]. The latent variables are generated only once based on the observations, and a LSTM uses the same latent variables at each time step to generate trajectories.

Our approach uses a VAE architecture as well, but the latent variables are generated along a time-dependent process during trajectory prediction. The main motivation behind our formulation is that human decision making is highly dynamic and can lead to different trajectories at any given time. As such, we introduce a timewise VAE architecture which we combine with RNNs for stochastic trajectory prediction.

**Stochastic RNNs for Sequential Modeling.** RNNs have been widely used to handle sequential data in deep learning applications. To better model highly dynamic and multimodal data, a number of works leverage a VAE architecture to extend RNNs with sequentially generated stochastic latent variables [33–36]. Besides employing different training tricks such as different loss function terms to encourage diversity or to approximate better the posterior distribution, the major differences among these works are the way the posterior approximation is parameterized and how the latent variables are used for prediction.

Though achieving SOTA results in general sequential data modeling tasks, timewise VAE methods with RNN structures do not consider the characteristic features of human navigation tasks. To better extract navigation features from observations, our approach encodes neighbors through a social-feature attention mechanism that uses social features similar to [31] to compute attention scores. However, instead of using RNN hidden states as the representation of neighbors’ states, we employ the actual, observable neighbor states (position and velocity) for synthesis, while the hidden state passed through the RNN are considered as internal states observable only by the target agent itself. Additionally, our posterior approximation takes the whole ground-truth (GT) trajectory into account through the use of bi-directional RNNs for better navigation pattern extraction.

## III. APPROACH

Our model infers the distribution of future trajectories for each agent in a scene, based on the social features extracted from historical observations. Specifically, given a scene containing  $N$  agents, let  $\mathbf{x}_i^t \in \mathbb{R}^2$  denote the the 2D spatial coordinate of each agent  $i$  at time step  $t$ . We perform  $H$ -frame inference for the distribution over future positions  $\mathbf{x}_i^{T+1:T+H}$  based on a  $T$ -frame joint observation of the whole scene, i.e., we predict the distribution  $p(\mathbf{x}_i^{T+1:T+H} | \mathcal{O}_i^{1:T})$  where  $\mathcal{O}_i^{1:T}$  is the set of local observations gathered from agent  $i$  to all the agents. We will give more details on how these observations  $\mathcal{O}_i^{1:T}$  is defined and encoded in Section III-B.

Our approach performs prediction for each agent independently based on social features extracted from the local observation, and can run with scenes having an arbitrary number of agents. The backbone of our model is a timewise VAE. In the following, we present our approach that we call SocialVAE.

### A. Model Architecture

Figure 1 shows the system overview of our model. Similarly to prior works [33–36], we use a RNN structure to condition the sequential predictions through an auto-regressive model relying on the state variable of the RNN structure. However, while such prior works directly perform predictions over time-sequence data, our model introduces the past observations as a conditional variable. Moreover, instead of directly predicting the absolute spatial coordinates  $\mathbf{x}_i^{T+1:T+H}$ , we generate a displacement sequence  $\mathbf{d}_i^{T+1:T+H}$  unrelated to the global positions of trajectories, where  $\mathbf{d}_i^{t+1} \triangleq \mathbf{x}_i^{t+1} - \mathbf{x}_i^t$ . The target

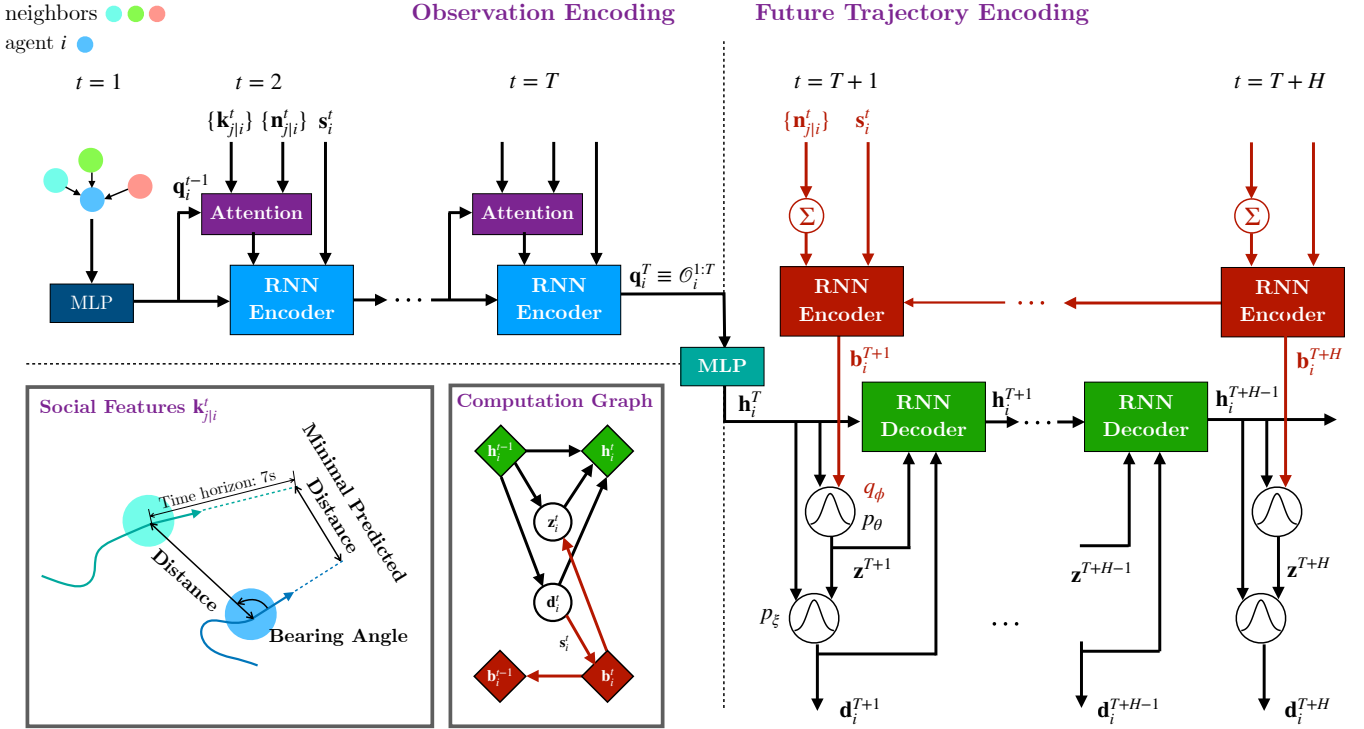


Fig. 1. Overview of SocialVAE architecture that employs a RNN-based timewise VAE with sequentially generated stochastic latent variables for trajectory prediction. During observation encoding (left), an attention mechanism is used that considers each neighbor’s state along with its corresponding social features. For trajectory decoding (right), a structured sequence of samples of latent variables is generated to produce the final trajectory. Red parts denote the computation during training where a bidirectional RNN is employed to capture the characteristics of the complete GT trajectory. Units with the same color share a network.

probability distribution of the displacement sequence can be written as

$$p(\mathbf{d}_i^{T+1:T+H} | \mathcal{O}_i^{1:T}) = \prod_{\tau=1}^H p(\mathbf{d}_i^{T+\tau} | \mathbf{d}_i^{T+1:T+\tau-1}, \mathcal{O}_i^{1:T}). \quad (1)$$

To generate stochastic predictions, we use a conditional prior over the RNN state variable to introduce latent variables at each time step, and thus obtain a timewise VAE architecture allowing us to model highly nonlinear dynamics during multi-agent navigation. In the following, we introduce our model by decomposing the VAE architecture into a generative model for trajectory prediction and an inference model for posterior approximation.

**Generative Model.** Let  $\mathbf{z}_i^t$  be the latent variables introduced at the time step  $t$ . To implement the sequential generative model  $p(\mathbf{d}_i^t | \mathbf{d}_i^{t-1}, \mathcal{O}_i^{1:T}, \mathbf{z}_i^t)$  we use a RNN in which the state variable  $\mathbf{h}_i^t$  is updated recurrently by

$$\mathbf{h}_i^t = \vec{g}(\psi_{\mathbf{z}\mathbf{d}}(\mathbf{z}_i^t, \mathbf{d}_i^t), \mathbf{h}_i^{t-1}) \quad (2)$$

for  $t = T + 1, \dots, T + H$ . The initial state at  $t = T$  is a function of the  $T$ -frame GT observation, i.e.

$$\mathbf{h}_i^T = \psi_{\mathbf{h}}(\mathcal{O}_i^{1:T}), \quad (3)$$

where  $\psi_{\mathbf{z}\mathbf{d}}$  and  $\psi_{\mathbf{h}}$  in Eqs. 2 and 3 are two embedding neural networks, respectively. Developing Eq. 1 with  $\mathbf{z}_i^t$ , we obtain

the generative model:

$$\begin{aligned} p(\mathbf{d}_i^{T+1:T+H} | \mathcal{O}_i^{1:T}) &= \prod_{t=T+1}^{T+H} \int_{\mathbf{z}_i^t} p(\mathbf{d}_i^t | \mathbf{d}_i^{T:t-1}, \mathcal{O}_i^{1:T}, \mathbf{z}_i^t) p(\mathbf{z}_i^t | \mathbf{d}_i^{T:t-1}, \mathcal{O}_i^{1:T}) d\mathbf{z}_i^t. \end{aligned} \quad (4)$$

In contrast to standard VAEs using a normal Gaussian distribution as the prior, our prior distribution is conditioned and can be obtained from the RNN state variable. For the second term of the integrals in Eq. 4, this translates into

$$p(\mathbf{z}_i^t | \mathbf{d}_i^{T:t-1}, \mathcal{O}_i^{1:T}) := p_{\theta}(\mathbf{z}_i^t | \mathbf{h}_i^{t-1}), \quad (5)$$

where  $\theta$  are parameters for a neural network that will be optimized. This results in a parameterized conditional prior distribution over the RNN state variable, through which we can track the distribution flexibly.

The first term of the integral in Eq. 4 implies sampling new displacements from the latent variable  $\mathbf{z}_i^t$  and from the observations and previous displacements captured by  $\mathbf{h}_i^{t-1}$ , i.e.

$$\mathbf{d}_i^t \sim p_{\xi}(\cdot | \mathbf{z}_i^t, \mathbf{h}_i^{t-1}), \quad (6)$$

with parameters  $\xi$ . Given the displacement definition  $\mathbf{d}_i^t$ , we obtain

$$\mathbf{x}_i^t = \mathbf{x}_i^T + \sum_{\tau=T+1}^t \mathbf{d}_i^{\tau}, \quad (7)$$

as a stochastic prediction of agent's  $i$  trajectory for  $t = T + 1, \dots, T + H$ .

**Inference Model.** To approximate the posterior  $q$  over the latent variables, we consider the whole trajectory over the GT observation  $\mathcal{O}_i^{1:T+H}$  to shape the latent variable distribution via a backward recurrent network [35, 36]:

$$\mathbf{b}_i^t = \overleftarrow{g}(\mathcal{O}_i^t, \mathbf{b}_i^{t+1}), \quad (8)$$

for  $t = T + 1, \dots, T + H$  given  $\mathbf{b}_i^{T+H+1} = \mathbf{0}$ . The state variable  $\mathbf{b}_i^t$  provides the GT trajectory information from  $t$  to  $T + H$ . By defining the posterior distribution as a function encoding both the backward state  $\mathbf{b}_i^t$  and forward state  $\mathbf{h}_i^t$ , the latent variable  $\mathbf{z}_i^t$  during inference is drawn implicitly based on the entire GT trajectory. With  $\phi$  the parameters of the network mapping  $\mathbf{b}_i^t, \mathbf{h}_i^{t-1}$  to the posterior parameters, we can sample through

$$\mathbf{z}_i^t \sim q_\phi(\cdot | \mathbf{b}_i^t, \mathbf{h}_i^{t-1}). \quad (9)$$

**Training.** Similarly to the standard VAE, the learning objective of our model is to maximize the evidence lower bound that sums up over all time steps given the target distribution defined in Eq. 4:

$$\sum_{t=T+1}^{T+H} \mathbb{E}_{\mathbf{z}_i^t \sim q_\phi(\cdot | \mathbf{b}_i^t, \mathbf{h}_i^{t-1})} [\log p_\xi(\mathbf{d}_i^t | \mathbf{z}_i^t, \mathbf{h}_i^{t-1})] - D_{KL} [q_\phi(\mathbf{z}_i^t | \mathbf{b}_i^t, \mathbf{h}_i^{t-1}) || p_\theta(\mathbf{z}_i^t | \mathbf{h}_i^{t-1})]. \quad (10)$$

To do so, we parameterize  $p_\xi$ ,  $q_\phi$  and  $p_\theta$  as multivariate Gaussian distributions using neural networks, i.e.

$$p_\xi := \mathcal{N}(\boldsymbol{\mu}_{i,d}^t, \boldsymbol{\Sigma}_{i,d}^t) \quad \text{with } [\boldsymbol{\mu}_{i,d}^t, \boldsymbol{\Sigma}_{i,d}^t] = \psi_\xi(\mathbf{z}_i^t, \mathbf{h}_i^{t-1}), \quad (11)$$

$$q_\phi := \mathcal{N}(\boldsymbol{\mu}_{i,\text{post}}^t, \boldsymbol{\Sigma}_{i,\text{post}}^t) \quad \text{with } [\boldsymbol{\mu}_{i,\text{post}}^t, \boldsymbol{\Sigma}_{i,\text{post}}^t] = \psi_\phi(\mathbf{b}_i^t, \mathbf{h}_i^{t-1}), \quad (12)$$

$$p_\theta := \mathcal{N}(\boldsymbol{\mu}_{i,\text{prior}}^t, \boldsymbol{\Sigma}_{i,\text{prior}}^t) \quad \text{with } [\boldsymbol{\mu}_{i,\text{prior}}^t, \boldsymbol{\Sigma}_{i,\text{prior}}^t] = \psi_\theta(\mathbf{h}_i^{t-1}), \quad (13)$$

where the distribution parameters are obtained through a decoder neural network  $\psi_\xi$ , an encoder neural network  $\psi_\phi$  and a feature extraction neural network  $\psi_\theta$  with parameters  $\xi$ ,  $\phi$  and  $\theta$  respectively. Performing optimization directly over the log-likelihood in Eq. 10 based on the GT value of  $\mathbf{d}_i^t$  ignores the accumulated error when we project  $\mathbf{d}_i^t$  back to  $\mathbf{x}_i^t$  using Eq. 7 to get the final trajectory. To address this issue, we replace the log-likelihood term with the squared error over  $\mathbf{x}_i^t$  and perform optimization over  $\mathbf{d}_i^t$  through reparameterization tricks [37]. By such a way, previous prediction errors are expected to be compensated in next predictions. The final loss to be minimized during training is

$$\mathbb{E}_i \left[ \frac{1}{H} \sum_{t=T+1}^{T+H} \mathbb{E}_{\substack{\mathbf{d}_i^t \sim p_\xi(\cdot | \mathbf{z}_i^t, \mathbf{h}_i^{t-1}) \\ \mathbf{z}_i^t \sim q_\phi(\cdot | \mathbf{b}_i^t, \mathbf{h}_i^{t-1})}} \left[ \left\| (\mathbf{x}_i^t - \mathbf{x}_i^T) - \sum_{\tau=T+1}^t \mathbf{d}_i^\tau \right\|^2 + q_\phi(\mathbf{z}_i^t | \mathbf{b}_i^t, \mathbf{h}_i^{t-1}) - p_\theta(\mathbf{z}_i^t | \mathbf{h}_i^{t-1}) \right] \right]. \quad (14)$$

For simplicity, at training, we sample  $\mathbf{z}_i^t$  and  $\mathbf{d}_i^t$  only once every time, and use the reparameterization trick of Gaussian distributions to update  $q_\phi$ ,  $p_\xi$  and  $p_\theta$ .

## B. Observation Encoding

In a  $N$ -agent scene, we define the local observation from agent  $i$  to the whole scene at time step  $t = 2, \dots, T$  as a vector containing the observation to the agent itself and the synthesis of all its neighbors:

$$\mathcal{O}_i^t := \left[ f_s(\mathbf{s}_i^t), \sum_j w_{j|i}^t f_n(\mathbf{n}_{j|i}^t) \right], \quad (15)$$

where

- $\mathbf{s}_i^t := [\mathbf{d}_i^t, \mathbf{d}_i^t - \mathbf{d}_i^{t-1}] \in \mathbb{R}^4$  is the self state of agent  $i$ , including the agent's velocity and acceleration information represented by position displacement,
- $\mathbf{n}_{j|i}^t := [\mathbf{x}_j^t - \mathbf{x}_i^t, \mathbf{d}_j^t - \mathbf{d}_i^t] \in \mathbb{R}^4$  is the local state of the neighbor agent  $j$  relative to agent  $i$ , including its relative position and velocity,
- $f_s$  and  $f_n$  are learnable feature extraction functions implemented through neural networks, and
- $w_{j|i}^t$  is an attention weight through which features from an arbitrary number of neighbors are fused together into a fixed-length vector.

Neighbors are re-defined at every time step. An agent  $j$  is considered as a neighbor of agent  $i$  at time step  $t$  if  $j \neq i$  and  $\|\mathbf{x}_j^t - \mathbf{x}_i^t\| < r_i$  where  $r_i$  is the maximal observation range of agent  $i$ . Non-neighbor agents are considered unobservable by agent  $i$ , and thus are ignored when we compose the local observation  $\mathcal{O}_i^t$ .

Note that we use the attention mechanism only for past observations  $t \leq T$ . In the case of the backward recurrent network used in Eq. 8, we simply set  $w_{j|i}^t = 1$  for all neighbors to form  $\mathcal{O}_i^t$  for  $t > T$ . To represent the past observation sequence while embedding the target agent's navigation strategy, we employ a RNN to encode the observations sequentially via its state variable, i.e.  $\mathcal{O}_i^{1:t} := \mathbf{q}_i^t$ , where the state variable  $\mathbf{q}_i^t$  is updated recurrently by

$$\mathbf{q}_i^{t+1} = g(\mathcal{O}_i^{t+1}, \mathbf{q}_i^t). \quad (16)$$

The initial state is extracted from the agent's and its neighbors' initial positions in the scene at the time step  $t = 1$ :

$$\mathbf{q}_i^1 = \sum_j f_{\text{init}}(\mathbf{x}_j^1 - \mathbf{x}_i^1) \quad (17)$$

where  $f_{\text{init}}$  is a neural network for feature extraction.

The attention weights,  $w_{j|i}^t$ , are obtained by a graph attention mechanism [38], which encodes node features by learnable edge weights. In detail, to synthesize neighbors in the scene at time step  $t$  using attention weights based on the observation from agent  $i$ , we regard the agent  $i$  and all its neighbors as nodes in a graph with directed edges from the neighbor nodes towards the agent node. Attention weights corresponding to the edge weights are computed by

$$w_{j|i}^t = \frac{\exp(e_{j|i}^t)}{\sum_{k \neq i} \exp(e_{k|i}^t)}, \quad (18)$$

where  $e_{j|i}^t$  is the weight of the edge from the neighbor node  $j$  to the agent node  $i$ . Let  $\mathbf{k}_{j|i}^t$  be the social features of neighbor  $j$  observed by agent  $i$ , which we explain later, and  $\mathbf{q}_i^{t-1}$  as defined above the navigation feature that agent  $i$  exhibits till the time step  $t$ . We obtain the edge weight through the cosine similarity between the agent's navigation feature and its neighbor's social features:

$$e_{j|i}^t = \text{LeakyReLU}(f_q(\mathbf{q}_i^{t-1}) \cdot f_k(\mathbf{k}_{j|i}^t)), \quad (19)$$

where  $f_q$  and  $f_k$  are neural networks embedding the features. This leads to a dot-product attention result using social features to synthesize neighbors while modeling the observation of an agent as a graph. In this attention scheme,

$$\sum_j w_{j|i}^t f_n(\mathbf{n}_{j|i}^t) \equiv \text{Attention}(\mathbf{q}_i^{t-1}, \{\mathbf{k}_{j|i}^t\}, \{f_n(\mathbf{n}_{j|i}^t)\}), \quad (20)$$

where  $\mathbf{q}_i^{t-1}$ ,  $\{\mathbf{k}_{j|i}^t\}$  and  $\{f_n(\mathbf{n}_{j|i}^t)\}$  respectively correspond to the query, key and value vectors in the vanilla attention mechanism. (cf. Fig 1).

As in the prior work [31], we define the social features of a neighbor  $j$  observed by the agent  $i$  at time step  $t$  as  $\mathbf{k}_{j|i}^t$  using three geometric features:

- the Euclidean distance between agents  $i$  and  $j$ , i.e.  $\|\mathbf{p}_{j|i}^t\|$  where  $\mathbf{p}_{j|i}^t = \mathbf{x}_j^t - \mathbf{x}_i^t$ ;
- the cosine value of the bearing angle from agent  $i$  to neighbor  $j$ , i.e.  $\cos(\mathbf{p}_{j|i}^t, \mathbf{d}_i^t)$ ;
- the minimal predicted distance [39] from agent  $i$  to  $j$  within a time horizon  $h$ , i.e.  $\|\mathbf{p}_{j|i}^t + \text{clip}(\tau, h)\mathbf{v}_{j|i}^t\|$  where  $\mathbf{v}_{j|i}^t = (\mathbf{d}_j^t - \mathbf{d}_i^t)/\Delta t$ ,  $\tau = -(\mathbf{p}_{j|i}^t \cdot \mathbf{v}_{j|i}^t)/\|\mathbf{v}_{j|i}^t\|^2$ , and  $\Delta t$  is the sampling interval between two frames.

In contrast to prior works [16, 18, 31] applying attention or attention-like mechanisms only on the last frame of the given observation sequence, our approach computes attention at every time step for better extracting the agent’s navigation strategy while always taking into account the social influence from its neighbors. In addition, we include the minimal predicted distance as an extra feature as it has been shown to accurately capture the anticipatory nature of human-human interactions [40–42].

#### IV. EXPERIMENTS

In the following, we first give details on the implementation and on the metrics used for evaluation, then we report and analyze experiments on two standard datasets: ETH/UCY [11, 43] and SDD [44], and on the SportVU NBA dataset [45, 46].

**Implementation details.** Our approach uses a local observation encoding and ignores agents’ global coordinates. To eliminate the global moving direction preferences in specific scenarios, we apply two types of data augmentation: scenario flipping and rotation. The training data is randomly flipped along x- and y-axis and rotated by some degree before fed into the network. We employ GRUs [47] with 256 units as the RNN structure. The slope of the LeakyReLU activation layer is 0.2. The observation range  $r_i$  is 2m for all pedestrians during training and evaluation. The horizon  $h$  used for the minimal predicted distance is 7s. The latent variable  $\mathbf{z}_i^t$  is modeled as a 32-dimensional, Gaussian-distributed variable. All training used 50,000 optimization iterations with a batch size of 128. We refer to <https://github.com/xupeio610/SocialVAE> for our implementation source code along with details on hyperparameters and pre-trained models.

**Evaluation Metrics and Baselines.** To evaluate our approach, we consider a deterministic prediction method, *Linear*, and five stochastic prediction baselines which are the current state-of-the-art baselines for pedestrian trajectory prediction in human-human interaction settings. These include SocialGAN [16], SoPhie [18], SocialWays [31], PECNet [19], and Trajectron++ [21]. Following the literature, we use three metrics to evaluate model performance:

- *Average Displacement Error* (ADE), the Euclidean distance between a prediction trajectory the Euclidean distance between a prediction trajectory  $\{\mathbf{x}_i^t\}$  and the GT value  $\{\hat{\mathbf{x}}_i^t\}$  averaged over all prediction frames for  $t = T + 1, \dots, T + H$ :

$$\text{ADE}(\{\mathbf{x}_i^t\}, \{\hat{\mathbf{x}}_i^t\}) = \frac{1}{H} \sum_{t=T+1}^{T+H} \|\mathbf{x}_i^t - \hat{\mathbf{x}}_i^t\|. \quad (21)$$

- *Final Displacement Error* (FDE), the Euclidean distance between the predicted position in the final frame and the corresponding GT value:

$$\text{FDE}(\{\mathbf{x}_i^t\}, \{\hat{\mathbf{x}}_i^t\}) = \|\mathbf{x}_i^{T+H} - \hat{\mathbf{x}}_i^{T+H}\|. \quad (22)$$

- *Negative Log Likelihood* (NLL), the negative logarithm of the value of the predictive PDF at GT trajectories. The predictive distribution is obtained by Gaussian kernel density estimation

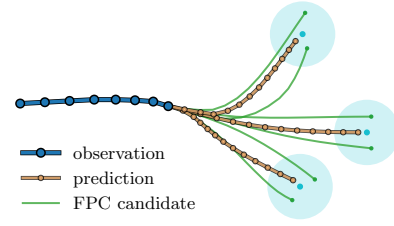


Fig. 2. An example of FPC to extract 3 predictions (orange) from 9 samples. The blue denotes the observed trajectory. The green denotes the other 6 samples besides the chosen ones. The cyan regions show the clustering result on the final positions of the 9 sample trajectories. The chosen predictions are the ones with final positions closest to the cluster centroids (cyan dots).

from 2,000 samples. For simplicity, distributions at each time step are estimated independently and we use the joint distributions to compute PDF values.

We compare ADEs and FDEs of our approach to the ones from the baselines by using 8 observation frames (3.2s) and 12 prediction frames (4.8s), i.e.  $T = 8$  and  $H = 12$ . The results are averaged over all tested trajectories. For stochastic baselines, we follow the methodology in most baselines and report the best prediction out of 20 predictions, i.e., for each GT trajectory, we do 20 predictions and keep the lowest ADEs and FDEs.

**SocialVAE with FPC.** Given that 20 predictions are a quite small batch of samples, our SocialVAE results are likely to be biased, as some samples may fall into low-density regions or all samples may be concentrated in high-density regions. As such, we propose a *final position clustering* (FPC) variant to our method in order improve the prediction diversity within a limited number of samples. With FPC, we do predictions more times than the desired number of samples (5 times in our experiments), and run a  $K$ -means clustering on the final positions of all the predicted trajectories to extract the desired number of  $K$  predictions (20 in our experiments). For each of the  $K$  clusters, we keep only the predicted trajectory whose final position is the closest to the cluster’s mean final position, and generate  $K$  predictions in total as the final result. Figure. 2 gives an example of FPC. where we pick 3 predicted trajectories out of 9 samples.

FPC is similar to the test-time sampling trick proposed in Y-Net [26]. However, Y-Net requires 10,000 samples for clustering to cover as many potential goal positions as possible, while our approach uses very few samples to bring performance improvement. It also demonstrates that our approach can provide a high-quality estimation to the trajectory distribution using a limited number of samples, rather than enumerating all possible candidate trajectories. We refer to Appendix II for sensitive analysis of FPC with varying sampling rates.

##### A. Experiments on ETH/UCY

We first evaluate our approach on the ETH/UCY benchmark [11, 43]. These datasets contain 1,536 pedestrian trajectories recorded in five different scenes, with rich interaction behaviors, including collision avoidance, group navigation, group merging and splitting. We use the same data preprocessing and evaluation methods with prior works on human trajectory prediction tasks [16, 18, 21, 31] and perform prediction in world coordinates. For evaluation, we apply a 5-fold cross validation where we train the model on data from four scenes and evaluate on the holdout scene.

Table I shows the corresponding ADE/FDE results obtained using the best of 20 predictions, and Table II shows the NLL given distributions obtained by Gaussian kernel density estimation from 2000 prediction samples. The ADE/FDE results are reported in the unit of meters. The reported results of SocialGAN and Trajectron++ were reproduced using their official implementations, which are slightly different from the results reported in the original papers. For

TABLE I  
ADE/FDE ON ETH/UCY BENCHMARK

	Linear	SocialGAN [16]	SoPhie [18]	SocialWays [31]	PECNet [19]	Trajectron++ [21]	SocialVAE	SocialVAE+FPC
<b>ETH</b>	1.07/2.28	0.63/1.09	0.70/1.43	<b>0.39/0.64</b>	0.54/0.87	0.54/0.94	0.49/0.77	0.46/0.70
<b>Hotel</b>	0.31/0.61	0.46/0.98	0.76/1.67	0.39/0.66	0.18/0.24	0.16/0.28	0.15/0.24	<b>0.14/0.21</b>
<b>Univ</b>	0.52/1.16	0.56/1.18	0.54/1.24	0.55/1.31	0.35/0.60	0.28/0.55	0.25/0.47	<b>0.23/0.40</b>
<b>Zara01</b>	0.42/0.95	0.33/0.67	0.30/0.63	0.44/0.64	0.22/0.39	0.21/0.42	0.19/0.37	<b>0.18/0.32</b>
<b>Zara02</b>	0.32/0.72	0.31/0.64	0.38/0.78	0.51/0.92	0.17/0.30	0.16/0.31	0.15/0.28	<b>0.13/0.24</b>

TABLE II  
NLL ON ETH/UCY BENCHMARK

	Trajectron++	SocialVAE
<b>ETH</b>	2.26	<b>0.96</b>
<b>Hotel</b>	-0.52	<b>-1.41</b>
<b>Univ</b>	0.32	<b>-0.49</b>
<b>Zara01</b>	-0.05	<b>-0.65</b>
<b>Zara02</b>	-1.00	<b>-2.67</b>

TABLE III  
ADE/FDE AND NLL ON STANFORD DRONE DATASET (SDD)

	PECNet	Trajectron++	SocialVAE	SocialVAE+FPC
ADE/FDE (m) <sup>a</sup>	-	1.35/2.05	0.30/0.50	<b>0.28/0.43</b>
ADE/FDE (p) <sup>b</sup>	9.29/15.93	-	9.08/14.78	<b>8.47/12.95</b>
NLL	-	1.76	<b>-0.43</b>	

<sup>a</sup> (m) is measured in meters; <sup>b</sup> (p) is measured in pixels.

SoPhie, SocialWays, and PECNet, the ADEs/FDEs of the original papers are reported. As it can be seen from the results, the linear model cannot effectively capture the complex movement patterns of pedestrians leading to high errors, though some of its results are better than the GAN-based baselines of SocialGAN, SoPhie and SocialWays [48]. Compared to the linear model and GAN-based baselines, PECNet, Trajectron++ and our approach clearly obtain better results, except for the ETH test case where SocialWays outperforms all other methods. Besides the attention mechanism described in Section III-B, the major difference of our approach from PECNet and Trajectron++ is that we introduce a timewise VAE architecture, while both PECNet and Trajectron++ use a conditional-VAE structure. Compared to PECNet and Trajectron++, SocialVAE leads to lower ADE and FDE values in all test cases. We can also see the improvement brought from FPC. Without FPC, the improvement of SocialVAE over Trajectron++ on ADE is about 8%, and 14% on FDE. With FPC applied, SocialVAE brings an improvement of about 16% and 25% in ADE and FDE, respectively, over Trajectron++ and of 52% and 59%, respectively, over SocialGAN. Overall, our approach significantly outperforms other baselines in 58/60 test cases. In the ETH scene, pedestrians move at a much faster speed and may be out-of-distribution data for the other four scenes. This could be a reason why SocialVAE does not perform that well on ETH as compared to SocialWays, though still outperforming the rest of the baselines.

To highlight the quality of our approach’s stochastic predictions, we show ADE, FDE and NLL distributions of all trajectories for each test case in Fig. 3. It can be clearly seen that our approach outperforms the previous state-of-the-art method, Trajectron++, in all test cases, exhibiting smaller maximal errors in both ADE and FDE evaluations, and smaller maximal values of NLL. Our approach shows smaller deviations and provides predictions closer to ground truth overall. The NLL distributions show that the SocialVAE predictive distributions have superior quality, with higher probability on the GT trajectories. We also note a clear improvement when FPC is applied, which demonstrates that FPC can help obtain better distributed predictions with a limited number of samples to cover the stochastic movement patterns of pedestrians.

### B. Experiments on SDD

The SDD dataset [44] includes 5,232 pedestrian trajectories in eight different scenes. To perform comparisons with SOTA methods, we have used the TrajNet [49] split to perform the training/testing processes. In Table III, we present similar mean ADE/FDE and NLL results on the SDD dataset altogether with comparisons with

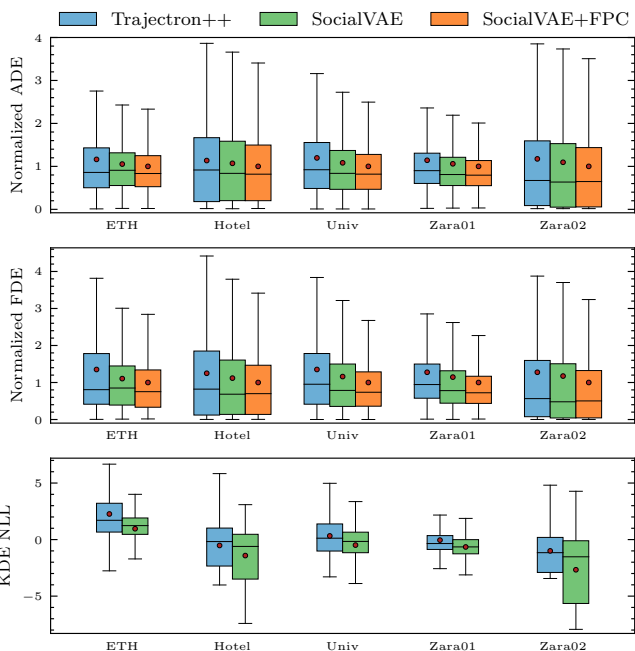


Fig. 3. Distributions of three metrics: ADE, FDE and NLL. The ADEs and FDEs are obtained from the best of 20 predictions, and normalized by the mean values of SocialVAE+FPC reported in Table I. NLL are computed from the distributions obtained by Gaussian kernel density estimation using 2,000 prediction samples.

reported results from PECNet and Trajectron++. The improvement with respect to these two state of the art approaches is significant in the three evaluated metrics. Note that for these comparisons, we report the ADE/FDE errors in meters and image pixels. Also, we have considered the Trajectron++ scores as reported by [50].

### C. Experiments on SportVU NBA Datasets

To test our approach on scenarios with more complex and intensive human-human interactions, we have extracted two sub-datasets, **Scoring** and **Rebounding**, from the SportVU basketball movement dataset [46, 50] focusing on games from the 2015-2016 NBA regular season. For each dataset, scenes are randomly split into testing and training sets using a 1:4 ratio. We refer to Appendix I for

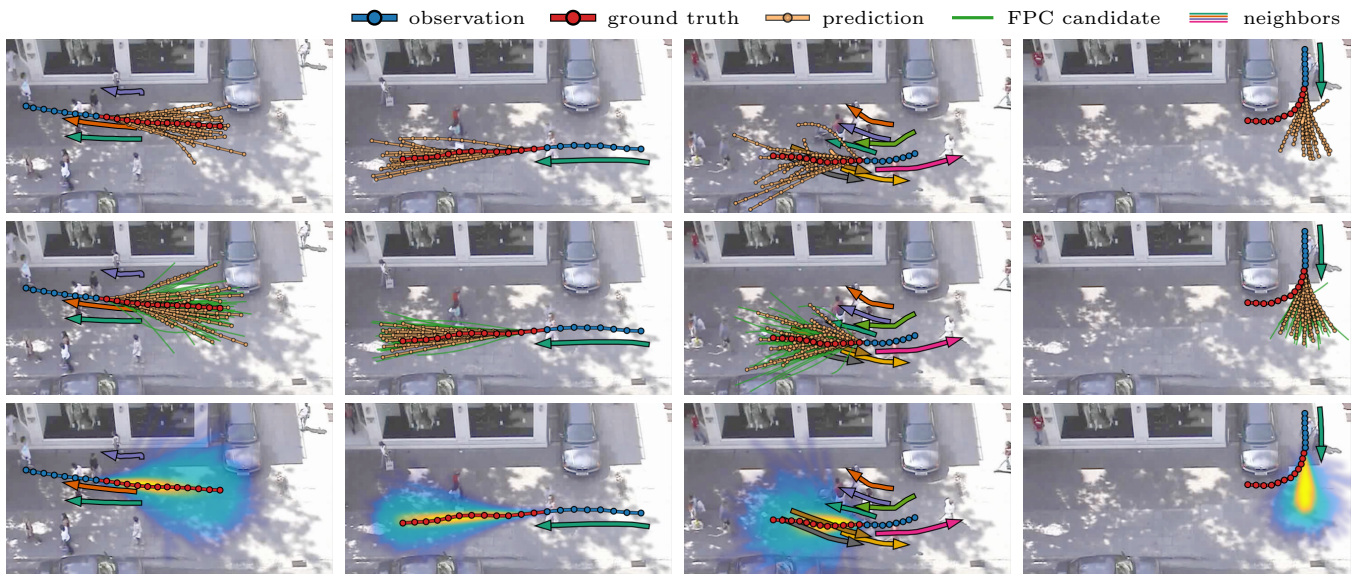


Fig. 4. Examples of predictions from SocialVAE. Observed trajectories are shown in blue, predicted trajectories are shown in orange, and GT is shown in red. Each column shows one scenario in the Zara scene with different prediction sampling methods. From top to bottom: SocialVAE without FPC, SocialVAE+FPC, and heatmaps of the predicted trajectory distribution. Heatmaps are generated using 2,000 samples.



Fig. 5. Attention maps at the 1st (left) and 20th (right) frames in the UCY *students003* dataset. Trajectories of pedestrians under prediction appear in blue. The other colored lines with arrows are the observed neighboring trajectories labeled in the dataset. Yellow dot denotes stationary neighbors who keep standing still during observation.

TABLE IV  
MODEL PERFORMANCE ON SPORTVU NBA DATASET

Scoring	Trajnetron++	SocialVAE	SocialVAE+FPC
ADE/FDE (m)	0.68/1.57	0.22/0.42	<b>0.21/0.37</b>
NLL	2.41		<b>1.90</b>
Rebounding	Trajnetron++	SocialVAE	SocialVAE+FPC
ADE/FDE (m)	0.26/0.54	0.20/0.37	<b>0.19/0.32</b>
NLL	2.69		<b>1.67</b>

the implementation details of data acquisition and model training.

Table IV reports the performance of our model on the testing sets in the two datasets. The original data were recorded in the unit of feet. Here we report the results in meters. We note that the overall frequency and nature of adversarial and cooperative interactions in the NBA dataset are significantly different from the ones in ETH/UCY and SDD datasets, which makes trajectory prediction a rather challenging problem as discussed in recent work [50]. As shown in the table, however, our approach achieves low errors on both datasets, which is significantly better than ones reported in prior work [50], though, it is unclear what training/testing data such works have used. Hence, we also report our own comparisons to Trajnetron++ in the table. Similar to the traditional ETH/UCY and

SDD datasets, SocialVAE exhibits state-of-the-art performance on the two SportVU NBA datasets. We also provide case study to qualitatively evaluate the model performance on the NBA datasets in Appendix I.

## V. ANALYSIS AND DISCUSSION

**Qualitative Evaluation.** Figure 4 compares trajectories generated by our approach with and without FPC in the Zara scene. We take the same approach as in our quantitative evaluation, and do a 12-frame prediction based on a 8-frame observation. To better understand the trajectories predictive distributions, besides generating 20 predictions with and without FPC, we also show the overall predictive distributions in the 3rd row of Fig. 4 by sampling 2,000 predictions. The distribution heatmaps clearly cover the GT trajectories very well, even in complex scenarios with lots of human-human interactions like the ones shown in the 3rd column. Though SocialVAE without FPC already generates predictions close to the GT trajectories, SocialVAE+FPC provides more diverse results to approximate the distributions better. In the 4th column scenario, for example, the pedestrian changes his direction in a way that cannot be captured from the 8-frame observation during which the pedestrian keeps walking on a straight line. Though the GT trajectory in this case is rather far from the mean of the predictive distribution, SocialVAE+FPC still provides a result quite close to the GT trajectory. Besides improving the diversity of predictions, FPC helps in eliminating outliers. For example, the topmost trajectory

TABLE V  
ABLATION RESULTS IN THE FORMAT OF ADE/FDE

	ETH	Hotel	Univ	Zara01	Zara02
SocialVAE	<b>0.49/0.77</b>	<b>0.15/0.24</b>	<b>0.25/0.47</b>	<b>0.19/0.37</b>	<b>0.15/0.28</b>
w/o timewise latents	0.50/0.88	0.16/0.27	0.26/0.50	0.20/0.39	<b>0.15/0.31</b>
w/o backward posterior	0.66/0.85	0.18/0.25	0.36/0.51	0.28/0.39	0.22/0.31
SocialVAE+FPC	<b>0.44/0.70</b>	<b>0.14/0.21</b>	<b>0.23/0.40</b>	<b>0.18/0.32</b>	<b>0.14/0.24</b>
w/o timewise latents	0.48/0.73	0.15/0.25	<b>0.23/0.42</b>	<b>0.18/0.34</b>	<b>0.14/0.28</b>
w/o backward posterior	0.63/0.72	0.18/0.22	0.35/0.44	0.27/0.34	0.22/0.27

samples in the 2nd and 3rd columns and the rightmost one in the 4th column are sampled from low-probability regions of the prediction distributions and are eliminated by FPC.

The predicted trajectories also show social characteristics. For example, in the 1st column, predictions for the individual walking alone show more multimodality compared to the pedestrian in the 2nd column who walks alongside another person. In the 3rd column, the predicted trajectories avoid collisions with the neighbors. On the other hand, since scene information is not part of our model local observation, SocialVAE ignores traversability and considers all regions accessible, which can lead to some unreasonable predictions. For example, the prediction distribution cover regions in the scene with cars parked.

**Attention.** Figure 5 shows how attention changes with the agents interactions. The top left neighbor who is too far away from the target pedestrian is ignored along with the idle neighbor (yellow dot). In the 1st frame (left two), much attention is paid to the green neighbor at the bottom who seems to be headed towards the pedestrian, while keeping an eye to the three neighbors on the right. In the 20th frame (right two), the model ignores the green neighbor as it has changed its direction, and shifts its attention to the three (red, purple, yellow) nearby neighbors. Among these neighbors, more attention is paid to the yellow agent on the left of the target pedestrian and less attention to the ones behind.

**Ablation Studies.** To understand what features in our proposed approach have a stronger impact on its performance, we perform ablation studies on two key features of SocialVAE: the use of timewise generated latent variables (Eq. 5) and the use of backward information from the GT trajectory to sample latent variables (Eq. 8). The results are presented in Table V. Both features seem to contribute to the overall improvement on the performance, with the second feature having more impact in ADE and both features leading to similar improvements in FDE. We refer to the supplementary material for additional results, including analysis on the FPC’s sampling rate and explanatory visualizations of the latent space.

## VI. CONCLUSION AND FUTURE WORK

We present SocialVAE as a novel approach for pedestrian trajectory prediction. It employs an attention-based mechanism to extract pedestrians’ navigation strategies from the social features exhibited in short-term observation, and relies on a timewise VAE architecture using RNN structures to generate stochastic predictions for future trajectories. We also introduce FPC, a clustering method based on the final positions of prediction trajectory samples, to extract a desired number of predictions from multiple samples for the sake of improving the diversity among a limited number of predictions. Our approach shows state-of-the-art performance in most of the test cases from the ETH/UCY and SDD trajectory prediction benchmarks. We also highlighted the applicability of SocialVAE to the non-traditional SportVU NBA data. To further improve the predictions quality and generate physically acceptable trajectories, an avenue for future work is extending the network structure and introducing semantic maps encoding the scene’s physical information as a part of the model input. By doing so, we hope to build a

model to take both human-space and human-agent interactions into account for prediction. This would also allow us to test SocialVAE on heterogeneous datasets involving different types of interacting agents [51, 52]. We further seek to extend our approach to enable end-to-end predictions allowing its deployment on physical agents such as indoor mobile robots.

## REFERENCES

- [1] A. Vaswani, N. Shazeer, N. Parmar, J. Uszkoreit, L. Jones, A. N. Gomez, L. Kaiser, and I. Polosukhin, “Attention is all you need,” *Advances in neural information processing systems*, vol. 30, 2017.
- [2] T. Brown, B. Mann, N. Ryder, M. Subbiah, J. D. Kaplan, P. Dhariwal, A. Neelakantan, P. Shyam, G. Sastry, A. Askell *et al.*, “Language models are few-shot learners,” *Advances in neural information processing systems*, vol. 33, pp. 1877–1901, 2020.
- [3] A. Van Oord, N. Kalchbrenner, and K. Kavukcuoglu, “Pixel recurrent neural networks,” in *International conference on machine learning*. PMLR, 2016, pp. 1747–1756.
- [4] A. Van den Oord, N. Kalchbrenner, L. Espeholt, O. Vinyals, A. Graves *et al.*, “Conditional image generation with pixelcnn decoders,” *Advances in neural information processing systems*, vol. 29, 2016.
- [5] S. Ravuri, K. Lenc, M. Willson, D. Kangin, R. Lam, P. Mirowski, M. Fitzsimons, M. Athanassiadou, S. Kashem, S. Madge *et al.*, “Skilful precipitation nowcasting using deep generative models of radar,” *Nature*, vol. 597, no. 7878, pp. 672–677, 2021.
- [6] J. A. Weyn, D. R. Durran, and R. Caruana, “Can machines learn to predict weather? using deep learning to predict gridded 500-hpa geopotential height from historical weather data,” *Journal of Advances in Modeling Earth Systems*, vol. 11, no. 8, pp. 2680–2693, 2019.
- [7] A. Sanchez-Gonzalez, J. Godwin, T. Pfaff, R. Ying, J. Leskovec, and P. Battaglia, “Learning to simulate complex physics with graph networks,” in *International Conference on Machine Learning*. PMLR, 2020, pp. 8459–8468.
- [8] D. Kochkov, J. A. Smith, A. Alieva, Q. Wang, M. P. Brenner, and S. Hoyer, “Machine learning–accelerated computational fluid dynamics,” *Proceedings of the National Academy of Sciences*, vol. 118, no. 21, 2021.
- [9] D. Helbing and P. Molnar, “Social force model for pedestrian dynamics,” *Physical review E*, vol. 51, no. 5, p. 4282, 1995.
- [10] D. Helbing, I. Farkas, and T. Vicsek, “Simulating dynamical features of escape panic,” *Nature*, vol. 407, no. 6803, pp. 487–490, 2000.
- [11] S. Pellegrini, A. Ess, K. Schindler, and L. Van Gool, “You’ll never walk alone: Modeling social behavior for multi-target tracking,” in *2009 IEEE 12th international conference on computer vision*. IEEE, 2009, pp. 261–268.
- [12] I. Karamouzas, B. Skinner, and S. J. Guy, “Universal power law governing pedestrian interactions,” *Physical Review Letters*, vol. 113, no. 23, p. 238701, 2014.
- [13] J. van den Berg, S. J. Guy, M. Lin, and D. Manocha, “Reciprocal n-body collision avoidance,” in *International Symposium of Robotics Research*, 2011, pp. 3–19.
- [14] N. Pradhan, T. Burg, and S. Birchfield, “Robot crowd navigation using predictive position fields in the potential function framework,” in *Proceedings of the 2011 American control conference*. IEEE, 2011, pp. 4628–4633.
- [15] A. Alahi, K. Goel, V. Ramanathan, A. Robicquet, L. Fei-Fei, and S. Savarese, “Social lstm: Human trajectory prediction in crowded spaces,” in *Proceedings of the IEEE conference on computer vision and pattern recognition*, 2016, pp. 961–971.



- [16] A. Gupta, J. Johnson, L. Fei-Fei, S. Savarese, and A. Alahi, "Social gan: Socially acceptable trajectories with generative adversarial networks," in *Proceedings of the IEEE Conference on Computer Vision and Pattern Recognition*, 2018, pp. 2255–2264.
- [17] A. Vemula, K. Muelling, and J. Oh, "Social attention: Modeling attention in human crowds," in *2018 IEEE International Conference on Robotics and Automation (ICRA)*. IEEE, 2018, pp. 4601–4607.
- [18] A. Sadeghian, V. Kosaraju, A. Sadeghian, N. Hirose, H. Rezatofghi, and S. Savarese, "Sophie: An attentive gan for predicting paths compliant to social and physical constraints," in *Proceedings of the IEEE/CVF Conference on Computer Vision and Pattern Recognition*, 2019, pp. 1349–1358.
- [19] K. Mangalam, H. Girase, S. Agarwal, K.-H. Lee, E. Adeli, J. Malik, and A. Gaidon, "It is not the journey but the destination: Endpoint conditioned trajectory prediction," in *European Conference on Computer Vision*. Springer, 2020, pp. 759–776.
- [20] B. Ivanovic and M. Pavone, "The trajctron: Probabilistic multi-agent trajectory modeling with dynamic spatiotemporal graphs," in *Proceedings of the IEEE/CVF International Conference on Computer Vision*, 2019, pp. 2375–2384.
- [21] T. Salzmann, B. Ivanovic, P. Chakravarty, and M. Pavone, "Trajctron++: Dynamically-feasible trajectory forecasting with heterogeneous data," in *Computer Vision—ECCV 2020: 16th European Conference, Glasgow, UK, August 23–28, 2020, Proceedings, Part XVIII 16*. Springer, 2020, pp. 683–700.
- [22] K. M. Kitani, B. D. Ziebart, J. A. Bagnell, and M. Hebert, "Activity forecasting," in *European conference on computer vision*. Springer, 2012, pp. 201–214.
- [23] L. Ballan, F. Castaldo, A. Alahi, F. Palmieri, and S. Savarese, "Knowledge transfer for scene-specific motion prediction," in *European Conference on Computer Vision*. Springer, 2016, pp. 697–713.
- [24] A. Sadeghian, F. Legros, M. Voisin, R. Vesel, A. Alahi, and S. Savarese, "Car-net: Clairvoyant attentive recurrent network," in *Proceedings of the European Conference on Computer Vision (ECCV)*, 2018, pp. 151–167.
- [25] Z. Cao, H. Gao, K. Mangalam, Q.-Z. Cai, M. Vo, and J. Malik, "Long-term human motion prediction with scene context," in *European Conference on Computer Vision*. Springer, 2020, pp. 387–404.
- [26] K. Mangalam, Y. An, H. Girase, and J. Malik, "From goals, waypoints & paths to long term human trajectory forecasting," in *Proceedings of the IEEE/CVF International Conference on Computer Vision*, 2021, pp. 15 233–15 242.
- [27] K. Yamaguchi, A. C. Berg, L. E. Ortiz, and T. L. Berg, "Who are you with and where are you going?" in *CVPR 2011*. IEEE, 2011, pp. 1345–1352.
- [28] J. M. Wang, D. J. Fleet, and A. Hertzmann, "Gaussian process dynamical models for human motion," *IEEE transactions on pattern analysis and machine intelligence*, vol. 30, no. 2, pp. 283–298, 2007.
- [29] P. Trautman and A. Krause, "Unfreezing the robot: Navigation in dense, interacting crowds," in *2010 IEEE/RSJ International Conference on Intelligent Robots and Systems*. IEEE, 2010, pp. 797–803.
- [30] K. Kim, D. Lee, and I. Essa, "Gaussian process regression flow for analysis of motion trajectories," in *2011 International Conference on Computer Vision*. IEEE, 2011, pp. 1164–1171.
- [31] J. Amirian, J.-B. Hayet, and J. Pettré, "Social ways: Learning multi-modal distributions of pedestrian trajectories with gans," in *Proceedings of the IEEE/CVF Conference on Computer Vision and Pattern Recognition Workshops*, 2019, pp. 0–0.
- [32] K. Sohn, H. Lee, and X. Yan, "Learning structured output representation using deep conditional generative models," *Advances in neural information processing systems*, vol. 28, pp. 3483–3491, 2015.
- [33] J. Bayer and C. Osendorfer, "Learning stochastic recurrent networks," *arXiv preprint arXiv:1411.7610*, 2014.
- [34] J. Chung, K. Kastner, L. Dinh, K. Goel, A. C. Courville, and Y. Bengio, "A recurrent latent variable model for sequential data," *Advances in neural information processing systems*, vol. 28, 2015.
- [35] M. Fraccaro, S. K. Sønderby, U. Paquet, and O. Winther, "Sequential neural models with stochastic layers," *Advances in neural information processing systems*, vol. 29, 2016.
- [36] A. Goyal, A. Sordoni, M.-A. Côté, N. R. Ke, and Y. Bengio, "Z-forcing: Training stochastic recurrent networks," *Advances in neural information processing systems*, vol. 30, 2017.
- [37] D. P. Kingma and M. Welling, "Auto-encoding variational bayes," in *International Conference on Learning Representations, ICLR 2014*, Y. Bengio and Y. LeCun, Eds., 2014.
- [38] P. Veličković, G. Cucurull, A. Casanova, A. Romero, P. Lio, and Y. Bengio, "Graph attention networks," *arXiv preprint arXiv:1710.10903*, 2017.
- [39] A.-H. Olivier, A. Marin, A. Créteil, and J. Pettré, "Minimal predicted distance: A common metric for collision avoidance during pairwise interactions between walkers," *Gait & posture*, vol. 36, no. 3, pp. 399–404, 2012.
- [40] J. Pettré, J. Ondřej, A.-H. Olivier, A. Cretual, and S. Donikian, "Experiment-based modeling, simulation and validation of interactions between virtual walkers," in *Proceedings of the 2009 ACM SIGGRAPH/Eurographics symposium on computer animation*, 2009, pp. 189–198.
- [41] M. Moussaïd, D. Helbing, and G. Theraulaz, "How simple rules determine pedestrian behavior and crowd disasters," *Proceedings of the National Academy of Sciences*, vol. 108, no. 17, pp. 6884–6888, 2011.
- [42] I. Karamouzas, N. Sohre, R. Hu, and S. J. Guy, "Crowd space: A predictive crowd analysis technique," *ACM Transactions on Graphics*, vol. 37, no. 6, 2018.
- [43] A. Lerner, Y. Chrysanthou, and D. Lischinski, "Crowds by example," in *Computer graphics forum*, vol. 26. Wiley Online Library, 2007, pp. 655–664.
- [44] A. Robicquet, A. Sadeghian, A. Alahi, and S. Savarese, "Learning social etiquette: Human trajectory understanding in crowded scenes," in *Proc. of the European Conf. in Computer Vision (ECCV)*, B. Leibe, J. Matas, N. Sebe, and M. Welling, Eds. Cham: Springer International Publishing, 2016, pp. 549–565.
- [45] K. Linou, D. Linou, and M. de Boer, "Nba player movements," <https://github.com/linouk23/NBA-Player-Movements>, 2016.
- [46] Y. Yue, P. Lucey, P. Carr, A. Bialkowski, and I. Matthews, "Learning fine-grained spatial models for dynamic sports play prediction," in *2014 IEEE International Conference on Data Mining*, 2014, pp. 670–679.
- [47] K. Cho, B. Van Merriënboer, C. Gulcehre, D. Bahdanau, F. Bougares, H. Schwenk, and Y. Bengio, "Learning phrase representations using rnn encoder-decoder for statistical machine translation," *arXiv preprint arXiv:1406.1078*, 2014.
- [48] C. Schöller, V. Aravntinos, F. Lay, and A. C. Knoll, "What the constant velocity model can teach us about pedestrian motion prediction," *IEEE Robotics Autom. Lett.*, vol. 5, no. 2, pp. 1696–1703, 2020.
- [49] S. Becker, R. Hug, W. Hübner, and M. Arens, "An evaluation of trajectory prediction approaches and notes on the trajnet benchmark," *CoRR*, vol. abs/1805.07663, 2018. [Online]. Available: <http://arxiv.org/abs/1805.07663>
- [50] O. Makansi, J. von Kügelgen, F. Locatello, P. V. Gehler, D. Janzing, T. Brox, and B. Schölkopf, "You mostly walk alone: Analyzing feature attribution in trajectory prediction," *CoRR*, vol. abs/2110.05304, 2021. [Online]. Available: <https://arxiv.org/abs/2110.05304>
- [51] H. Caesar, V. Bankiti, A. H. Lang, S. Vora, V. E. Liong, Q. Xu, A. Krishnan, Y. Pan, G. Baldan, and O. Beijbom, "nuscnets: A multimodal dataset for autonomous driving," in *IEEE/CVF Conference on Computer Vision and Pattern Recognition*, 2020, pp. 11 618–11 628.
- [52] R. Chandra, U. Bhattacharya, A. Bera, and D. Manocha, "Traffic: Trajectory prediction in dense and heterogeneous traffic using weighted interactions," *IEEE/CVF Conference on Computer Vision and Pattern Recognition*, 2019.

## APPENDIX I

### EXPERIMENTS ON SPORTVU NBA DATASET

Our analysis focuses on trajectory data of NBA games from the 2015–2016 regular season. Those data a rich set of lot of player-player interactions and highly non-linear motions. To evaluate our approach on such complex scenarios with intensive human-human interactions, we extracted two sub-datasets from the SportVU basketball movement dataset [46, 50]:

- 1) **Scoring dataset.** This dataset focuses on scenes involving a team scoring a basket. It contains a rich set of player-player interactions, both cooperative and adversarial, including highly non-linear player motions, set plays employed by different teams, and different offensive and defensive schemes.
- 2) **Rebounding dataset.** This dataset focuses on scenes involving a missed shot with players moving to grab the rebound. The dataset contains a number of interesting interactions, including players boxing out their opponents to allow a team

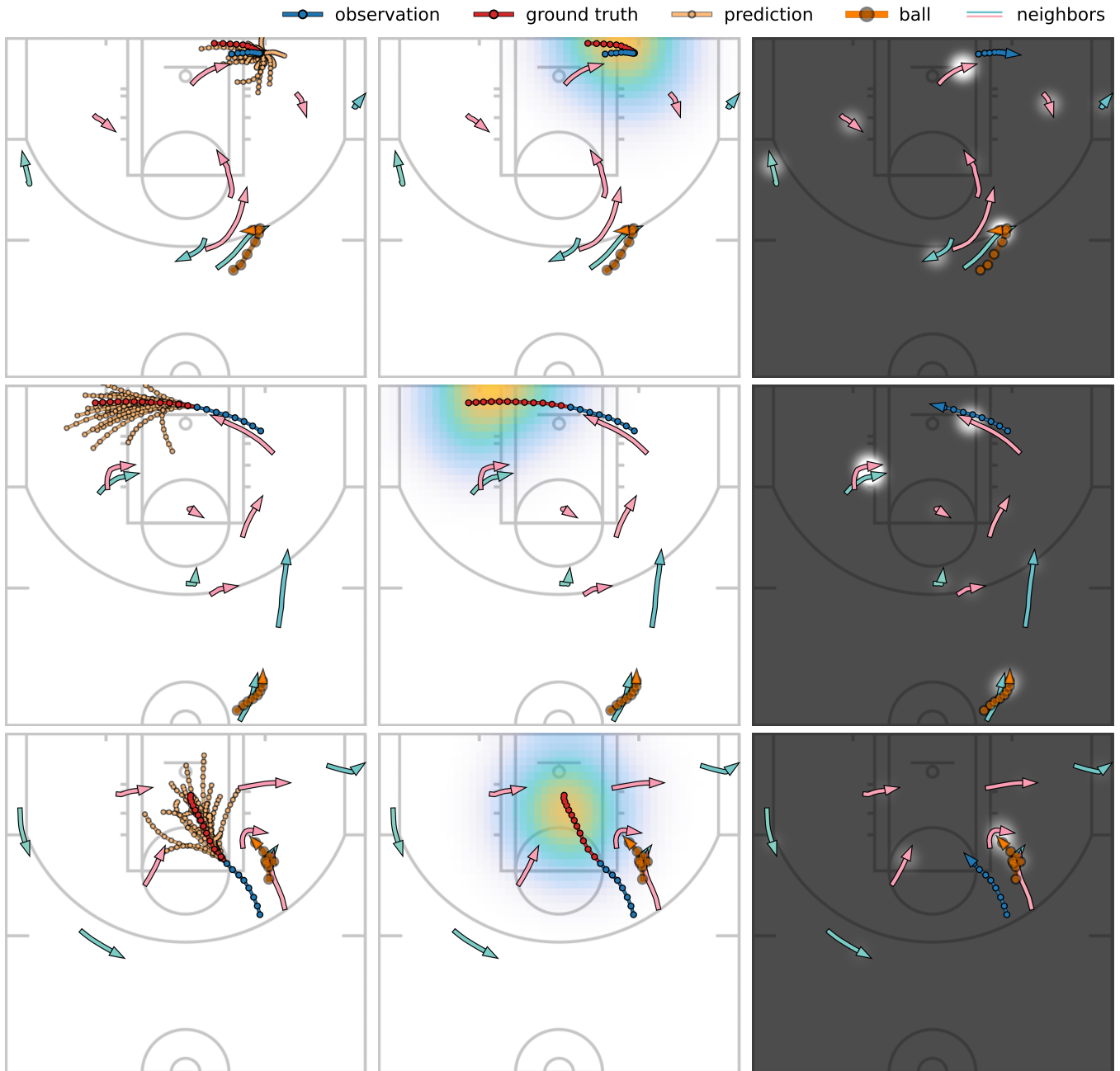


Fig. 6. Examples of trajectory predictions from SocialVAE on NBA SportVU datasets. From left to right: predicted trajectories, distribution heatmaps and attention maps. Azure lines with arrows identify trajectories of players who are in the same team with the one under prediction. Pink lines with arrows identify players from the opposite team. The orange indicates the ball trajectory.

member to grab a rebound, players moving towards the basket, and players starting to run on the other side of the half court for offensive or defensive purposes.

**Implementation Details and Results.** We refer to Table VI for detailed characteristics of the two datasets. Scenes are randomly split into testing and training sets using a 1:4 ratio for each dataset. The original data were recorded at 25 FPS. In consideration that basketball players move much faster than normal pedestrians, we downsample the data to the time interval of 0.12s (instead of 0.40s that we use on ETH/UCY and SDD benchmarks). We employ the same network structure that we have used for the ETH/UCY and SDD benchmarks (see Section III-A) and do 12-frame predictions for players (excluding the ball) based on 8-frame observations.

TABLE VI  
STATISTICAL INFORMATION ON SPORTVU NBA DATASETS.

	Scoring	Rebounding
# of Training/Testing Scenes	2,979/744	3,754/938
Avg. Play Duration (s)	11.82	2.94
# of Trajectories (20-frame)	2,958,480	257,230
Avg. Trajectory Length (m)	4.55	3.87

This leads to training and testing trajectories having 20 frames, with the average length around 4m, as reported in Table VI. The neighborhood radius  $r_i$  (see Section III-B), is set such that the

whole arena is covered, which means that all the players and the ball (projected on the ground) are taken into account when encoding historical observations and evaluating attention weights. The overall performance of our model on the two datasets is reported in Table IV.

**Qualitative Analysis.** Figure. 6 shows the predictions and attention maps in three testing scenarios. The scenarios exhibit rich interactions between players in both close and remote ranges. Players also show distinct movement patterns with fast heading direction changes and with speeds varying a lot given the same period of observation. Despite facing such complex behaviors, our model can still provide high-quality predictions. The predicted distributions cover the GT trajectories closely. As a challenging example shown in the 1st row in Fig. 6, our model successfully predicts the player’s strategic intention: he would change his moving direction sharply and seek opportunity to shake his marker and catch the ball. The predictive distribution gives several directions consistent with this strategic choice and covers well the one that the player effectively did. From the attention map, we can see that the model pays more attention to the defensive player who follows the one under prediction, and, across the range from the baseline to the three-point line, to the ball. Similar behaviors can be found in the examples shown in the 2nd and 3rd rows, where the player performs a fast move to create a passing lane and to crash the offensive board, respectively. Though we do not introduce any extra semantic information to indicate a ball neighbor to the model, the attention maps clearly show the effect produced by the ball to the player’s movement, even at a long distance. This means that our observation encoding approach, which relies on the social-feature attention mechanism, can effectively help the model identify the ball based on historical observations. We can also see that our model does not give the same attention to all players on the court but pays more to a subset of teammates and opponents who influence the predicted agent’s decision making. Furthermore, the predicted trajectories clearly exhibit multimodality, reflecting multiple possible responding behaviors that a player could take given the same scenario.

We let as a future work the introduction of semantic information such as the position on the court, the team id (teammates vs opponents), and the nature of the agent (human/ball).

## APPENDIX II SENSITIVITY ANALYSIS ON FPC

Our FPC implementation uses a sampling rate of  $\nu = 5$  by default. This means that, for 20 desired predictions, we run FPC on 100 samples. Figure 7 plots the ADE and FDE values when FPC is applied with varying values of  $\nu$  on the ETH/UCY benchmark, i.e., we run FPC on  $20\nu$  samples to produce 20 desired predictions. As shown in the figure, when the sampling rate increases from 1 to 5, there is a 10% to 15% improvement in FDE and a 5% improvement in ADE. However, increasing the sampling rate from 5 to 50 results in only about a 5% ADE/FDE improvement (with the exception of a 15% FDE improvement on ETH), at the cost though of 10 times the running time. This is probably due to the fact that as the multimodality becomes limited, when a minimal number of samples is attained, all the modes are covered with high probability. In any case, when running time does not matter, the performance of SocialVAE can be further improved by using FPC with a higher sampling rate.

## APPENDIX III LATENT SPACE ANALYSIS

To show that our model can learn a structured embedding of the observed trajectories, we plot the latent variable distributions in Fig. 8. To do so, we run a model pre-trained using the ETH/UCY datasets on 15 different 8-frame observations – a combination of five distinct trajectory headings and three distinct speeds. For each observation, we draw 150 samples of the latent variables from the prior at the first time step of prediction, which is generated directly

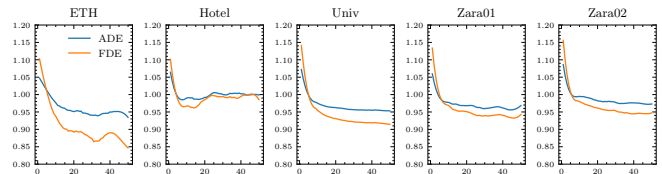


Fig. 7. Performance of FPC with respect to different sampling rates (1-50). All values are normalized by that of sampling rate 5 (default settings).

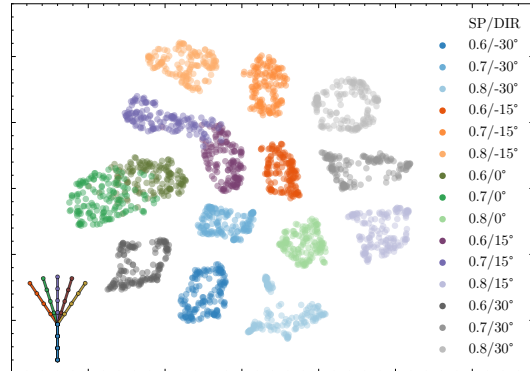


Fig. 8. t-SNE visualization of latent variable distributions given observation trajectories with different speeds (SP) and turn directions (DIR). The left bottom corner gives an example of the observed trajectories with different turn directions at the 5th frame from  $-30^\circ$  to  $30^\circ$ . For each of the five trajectory shapes, we consider observations with three constant speeds from 0.6m to 0.8m. This gives us a combination of 15 observations, as shown in the legend.

from the observation embedding (cf. Eq. 3 and 5). As it can be seen, our model can clearly distinguish observations with semantically different features.